RESEARCH PAPERS

Dust-cloud structures behind a shock wave moving over a deposited layer of fine particles*

WANG Boyi[1]**, XIONG Yi[1], CHEN Qian[1] and A. N. OSIPTSOV[2]

(1. LNM, Institute of Mechanics, Chinese Academy of Sciences, Beijing 100080, China; 2. Institute of Mechanics, Moscow State University, 119899 Moscow, Russia)

Received February 6, 2005; revised April 15, 2005

Abstract The present paper investigates dispersed-phase flow structures of a dust cloud induced by a normal shock wave moving at a constant speed over a flat surface deposited with fine particles. In the shock-fitted coordinates, the general equations of dusty-gas boundary layer flows are formulated within the framework of a multi-fluid model and parametric numerical studies of the carrier- and dispersed-phase flow fields are performed. The problem associated with crossing particle trajectories and the formation of local particle accumulation regions are solved by using the full Lagrangian method for the dispersed phase. The basic features of the near-wall two-phase flow under consideration including the role of Saffman force in the particle entrainment and the development of discontinuities or singularities in the particle density profiles are discussed. The effects associated with account of the non-uniformity of particle size and the finiteness of the particle Knudsen numbers are studied in detail.

Keywords: dust cloud, moving shock wave, particle entrainment, Knudsen effect, poly-disperse particles, full Lagrangian method.

A shock wave propagating over a deposited layer of fine particles may aerodynamically entrain the particles into the airflow and result in formation of a dust cloud behind the shock front. The knowledge of the height of particle rise and the particle distribution in this cloud is important for various practical applications, one of which is the prevention of dust fires and explosions in industry. Many organic or metallic powders (for example, cornstarch, coal, and aluminum) suspended in air form explosive mixtures. Dust explosions may occur if the initiation energy of the ignition source is high enough. Compared to gaseous mixtures, dust-air suspensions have extremely high explosion limits[1,2]. In addition, the high-speed particle-bed sweep-up problems are of interest not only for two-phase explosion and detonation but also for various natural phenomena such as tornadoes, intense dust storms and so on[3]. In this paper, we attempt to study the dispersed-phase flow patterns in the laminar flow region of a dusty-gas boundary layer induced by a normal shock wave travelling at a constant speed along a flat surface deposited with fine particles.

For laminar dusty-gas boundary layer flows[4], the main mechanism of transverse migration of particles is connected with the action of the shear-induced lifting force (usually called Saffman force). The rise of a particle from the surface of a deposit layer under the action of the Saffman force was considered in a number of previous studies[5—7]. However, only trajectories of an individual spherical particle initially located on a plane wall and set in motion by a shock wave were calculated in those papers. We have once performed a similar study[8] but only considered mono-disperse particles and neglected Knudsen effect in the momentum exchange between the phases. In the present work, we focus on conducting the parametric studies and examining the effects associated with the variation of the shock Mach number, the finiteness of the particle Knudsen number and the non-uniformity of the particle size (poly-dispersity). The action of the lifting and gravity forces on the particles in the boundary layer results in the appearance of crossing particle trajectories and the non-uniqueness of particle motion parameters. To overcome the difficulties of calculating the particle flow structures, we

* Supported by the National Natural Science Foundation of China (Grant No. 90205024) and Russian Foundation for Basic Research (RFBR Grant Nos. 05-01-00502 and 03-01-39004)

** To whom correspondence should be addressed. E-mail: wby@imech.ac.cn

developed the full Lagrangian approach, which is a Lagrangian variant of the method of characteristics. This approach makes it possible to calculate all the dispersed-phase parameters (including concentration) from systems of ordinary differential equations on foxed particle trajectories.

1 Formulation of the problem

We consider a two-dimensional laminar boundary-layer flow of a dusty gas, induced by a normal shock wave travelling along a flat surface deposited with fine particles. It is well known that in the neighborhood of the shock front, the flow is laminar down to the point of transition to turbulence[9]. When the shock wave velocity U_∞^* (or Mach number M) is constant, in the coordinates fitted to the shock front (Fig. 1), the two-phase flow is in a steady state.

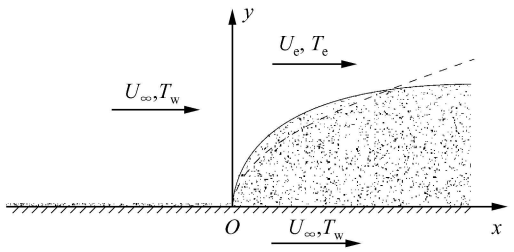

Fig. 1. Sketch of the gas boundary layer and the dust cloud induced by a moving shock wave over a deposited layer of fine particles. Solid line, upper boundary of the dust cloud; dashed line, outer edge of the gas boundary.

Usual assumptions of the dilute dusty gas model given by Marble[10] are adopted: (i) The carrier phase is a perfect viscous compressible gas; (ii) the dispersed phase consists of several (in general case m) fractions of solid spheres of radius σ_m^* and mass m_m^*; (iii) the Brownian motion, mutual collisions and the particle volume concentration are neglected and so each fraction of the dispersed phase can be treated as a zero-pressure fluid; (iv) there are no chemical reactions or phase transitions on the particle surface and so there is no mass transfer between the phases. Besides, we assume that the deposit layer on the wall consists of a loose material with m fractions of particles. In what follows, for simplicity, we will consider either mono-disperse ($m=1$) or bi-disperse ($m=2$) dust cloud resulting from the erosion of the deposit layer. The upper surface of the deposit layer is subject to steady-state erosion. For simplicity, we assume that the surface of the eroded layer remains plane aerodynamically and at each point of this surface a constant normal flux of the particle number concentration $N^* = n_{sw}^* v_{sw}^*$ is sustained. We also assume that the normal velocity of the particles leaving the surface tends to zero when approaching the eroded surface; in other words, we consider the purely aerodynamic entrainment due to the shear lifting force in this work.

For describing the interaction between the gas and the particles in the near-wall region, we will use the expressions for the drag, lifting force, and heat flux valid for a single sphere in a steady shear flow (below, the subscript s refers to the solid particles):

$$\boldsymbol{f}_s^* = 6\pi\sigma^*\mu^*(\boldsymbol{V}^* - \boldsymbol{V}_s^*)D - 6.46\sigma^{*2}(\rho^*\mu^*|\partial u^*/\partial y^*|)^{1/2} \cdot H(u^* - u_s^*)\boldsymbol{j}, \quad (1)$$

$$q_s^* = 4\pi\sigma^* k^*(T^* - T_s^*)G. \quad (2)$$

Here, $\boldsymbol{V}^*$, ρ^* and T^* are respectively the velocity vector (its components in x^*- and y^*-axis are u^* and v^*, respectively), density and temperature; μ^* and k^* are the gas viscosity and thermal conductivity while $\boldsymbol{j}$ is the unit vector along the y^*-axis. The correction functions D, G and H are introduced since, in the course of particle motion behind the shock wave, the characteristic particle Reynolds and Mach numbers may vary in a very wide range and, for fine particles, the deviations from the continuum flow should be also taken into account. For the drag force and the heat flux exerted on the particle, we will use the known approximate formulas[11,12] which cover the widest range of the flowing parameters:

$$D = (1 + Re_s^{2/3}/6)\phi,$$
$$\phi = (1 + \exp(-0.427M_s^{-4.63} - 3Re_s^{-0.88}))/\varphi,$$
$$\varphi = 1 + Kn_s(2.57 + 0.68\exp(-1.86/Kn_s)); \quad (3)$$

and

$$G = (1 + 0.3Pr^{1/3}Re_s^{1/2})/\psi,$$
$$\psi = 1 + 2.30Kn_s(1 + 0.3Pr^{1/3}Re_s^{1/2})/Pr. \quad (4)$$

For describing the shear-induced lifting force, we will use the approximate formula given by Mei[13] which generalizes the classical Saffman formula[14] and can be used both for small and finite (up to 100) particle Reynolds numbers:

$$H = 0.4687(1 - \exp(-0.1Re_s))(Re_g/Re_s)^{1/2} + \exp(-0.1Re_s), \quad (Re_s \leqslant 40),$$
$$H = 0.0741Re_g^{1/2}, \quad (Re_s > 40). \quad (5)$$

The total force and heat flux exerted on the dispersed

phase by the carrier phase is the sum of the forces and heat fluxes on a single sphere given above. In Eqs. (3)—(5), five dimensionless parameters are introduced: (a) The slip Reynolds number of the particle $Re_s = 2\sigma^* \rho^* | \boldsymbol{V}^* - \boldsymbol{V}_s^* | / \mu^*$; (b) the shear Reynolds number of the flow around the particle $Re_g = \sigma^{*2} \rho^* | \partial u^* / \partial y^* | / \mu^*$; (c) the slip Mach number of the particle $M_s = | \boldsymbol{V}^* - \boldsymbol{V}_s^* | / c^*$ (c^* is the gas speed of sound); (d) the Knudsen number of the particle $Kn_s = 1.255\sqrt{\gamma} M_s / Re_s$ (γ is the ratio of the gas specific heats); (e) the Prandtl number of the carrier gas $Pr = c_p^* \mu^* / k^*$ (here c_p^* is the specific heat at constant pressure).

To obtain the boundary layer equations, we introduce the stretched boundary-layer coordinate η and define the following dimensionless variables (below, the superscript $*$ and the subscript w refer respectively to the dimensional quantities and the wall parameters):

$$x = \frac{x^*}{l^*}, \quad \eta = \frac{y^*}{l^*}\sqrt{Re}, \quad u = \frac{u^*}{U_0^*},$$

$$v = \frac{v^*}{U_0^*}\sqrt{Re}, \quad u_s = \frac{u_s^*}{U_0^*}, \quad v_s = \frac{v_s^*}{U_0^*}\sqrt{Re},$$

$$T = \frac{T^*(U_\infty^* - U_0^*) + U_0^* T_w^* - U_\infty^* T_0^*}{(T_w^* - T_0^*)U_0^*},$$

$$T_s = \frac{T_s^*(U_\infty^* - U_0^*) + U_0^* T_w^* - U_\infty^* T_0^*}{(T_w^* - T_0^*)U_0^*},$$

$$\rho = \frac{\rho^*}{\rho_0^*}, \quad n_s = \frac{n_s^*}{n_s^0}, \quad p = \frac{p^*}{\rho_0^* U_0^{*2}}, \quad \mu = \frac{\mu^*}{\mu_0^*}.$$

Here, p and n_s are the gas pressure and particle number density, and the scale of the particle number density is equal to $n_s^0 = N^* \sqrt{Re} / U_0^*$. The other reference quantities (denoted by the subscript 0) are the gas flow parameters in the inviscid region immediately behind the shock front, related with the parameters ahead of the shock wave by the Rankine-Hugoniot conditions. In the formulas given above, two characteristic parameters are used: (a) The phase velocity relaxation length for the Stokes drag $l^* = m^* U_0^* / 6\pi\sigma^* \mu_0^*$; (b) the flow Reynolds number based on the velocity relaxation length $Re = \rho_0^* U_0^* l^* / \mu_0^*$.

We will write the equations of the laminar dusty-gas boundary layer over a moving flat plane in the shock-fitted coordinates (x, η) first for the case of mono-disperse particles (here the subscript m is omitted). The governing equations of the carrier phase take the following form:

$$\frac{\partial \rho u}{\partial x} + \frac{\partial \rho v}{\partial \eta} = 0, \tag{6}$$

$$\rho\left(u\frac{\partial u}{\partial x} + v\frac{\partial u}{\partial \eta}\right) = \frac{\partial}{\partial \eta}\left(\mu\frac{\partial u}{\partial \eta}\right) - \frac{\mathrm{d}p_e}{\mathrm{d}x} - Q, \tag{7}$$

$$\rho\left(u\frac{\partial T}{\partial x} + v\frac{\partial T}{\partial \eta}\right) = \frac{1}{Pr}\frac{\partial}{\partial \eta}\left(\mu\frac{\partial T}{\partial \eta}\right) + (a-1)Ec\left[\mu\left(\frac{\partial u}{\partial \eta}\right)^2 + u\frac{\mathrm{d}p_e}{\mathrm{d}x} + R\right] - S. \tag{8}$$

The state equation of the carrier phase takes the following form:

$$\rho\theta = \gamma M_0^2 p_e, \tag{9}$$

where the dimensionless function θ is defined as $\theta = [(d-1)T + a - d]/(a-1)$ and the gas pressure p_e at the outer edge of the boundary layer should be calculated from the solution of the outer problem of the relaxation region behind a planar shock wave. In Eqs. (6)—(8), the interphase coupling terms are given as

$$Q = \alpha\mu\sum_i n_{si}(u - u_{si})D_i,$$

$$R = \alpha\mu\sum_i n_{si}(u - u_{si})^2 D_i,$$

$$S = \alpha\mu(2/3Pr)\sum_i n_{si}(T - T_{si})G_i.$$

Here, in the term R, characterizing the work of the viscous forces at the relative displacement of the phases, the normal velocities v and v_s are neglected because their contributions are small compared to those of the longitudinal velocities u and u_s. In order to take into account the possibility of intersection of particle trajectories, we introduce as many one-velocity particle continua (denoted by the subscript i) as there are trajectories intersecting at the point of space (x, η) under consideration, where collisions between different continua can be neglected according to the adopted model of dilute dusty gas. In Eqs. (6)—(9), five dimensionless parameters are introduced:

$$\alpha = \frac{U_\infty^*}{U_0^*}, \quad d = \frac{T_w^*}{T_0^*}, \quad Ec = \frac{U_0^{*2}}{c_p^*(T_w^* - T_0^*)},$$

$$M_0 = \frac{U_0^*}{c_0^*}, \quad \alpha = \frac{m^* n_s^0}{\rho_0^*}.$$

When the wall temperature T_w^* is constant and equal to the gas temperature ahead of the shock front, by using the Rankine-Hugoniot relations, we can repre-

sent a, d, Ec and M_0 in terms of the specific heat ratio γ and the shock Mach number M:

$$a=\frac{(\gamma+1)M^2}{2+(\gamma-1)M^2},$$

$$d=\frac{(\gamma+1)^2M^2}{(\gamma+1)^2M^2+2(\gamma-1)(M^2-1)(1+\gamma M^2)},$$

$$Ec=-\left(\frac{\gamma-1}{d-1}\right)\left(\frac{2+(\gamma-1)M^2}{2\gamma M^2-(\gamma-1)}\right),$$

$$M_0^2=\frac{1+(\gamma-1)M^2/2}{\gamma M^2-(\gamma-1)/2}.$$

In the Eulerian form, the governing equations of a one-velocity continuum of the dispersed phase are (below the subscript i is omitted):

$$\frac{\partial n_s u_s}{\partial x}+\frac{\partial n_s v_s}{\partial \eta}=0, \tag{10}$$

$$u_s\frac{\partial u_s}{\partial x}+v_s\frac{\partial u_s}{\partial \eta}=\mu(u-u_s)D, \tag{11}$$

$$u_s\frac{\partial v_s}{\partial x}+v_s\frac{\partial v_s}{\partial \eta}=\mu(v-v_s)D-\kappa(u-u_s)H\left(\rho\mu\left|\frac{\partial u}{\partial \eta}\right|\right)^{1/2}-\omega, \tag{12}$$

$$u_s\frac{\partial T_s}{\partial x}+v_s\frac{\partial T_s}{\partial \eta}=\frac{2\chi\mu}{3Pr}(T-T_s)G. \tag{13}$$

Clearly, in Eqs. (10)—(13), other four dimensionless parameters are introduced:

$$\chi=\frac{c_p^*}{c_s^*},\quad \kappa=\frac{6.46}{12\pi\sqrt{6}}\left(\frac{2\rho_s^0}{\rho_0^*}\right)^{1/4}Re_0^{3/2},$$

$$\omega=\frac{g^*\sigma^*}{108U_0^{*2}}\left(\frac{2\rho_s^0}{\rho_0^*}\right)^{3/2}Re_0^2,\quad Re_0=\frac{2U_0^*\rho_0^*\sigma^*}{\mu_0^*}.$$

Here, c_s^* and ρ_s^0 are the specific heat and density of the particle material, g^* is the gravity force acceleration, Re_0 is the characteristic particle Reynolds number. The other Reynolds, Mach, and Knudsen numbers of the particle entering in D, G, H can be expressed in terms of κ and Re_0:

$$Re=\left(\frac{12\pi\kappa}{6.46Re_0}\right)^4,\quad Re_s=\frac{\rho|u-u_s|}{\mu}Re_0,$$

$$Re_g=\rho\mu\left|\frac{\partial u}{\partial \eta}\right|\left(\frac{3.23Re_0^2}{12\pi\kappa}\right)^2,$$

$$M_s=\frac{|u-u_s|}{(\gamma p/\rho)^{1/2}},\quad Kn_s=\frac{1.255\mu}{(p\rho)^{1/2}}Re_0^{-1}.$$

Similarly, the contributions of the normal velocities v and v_s are neglected in the Re_s and M_s expressions.

The boundary conditions for Eqs. (6)—(8) and (10)—(13) are specified just behind the shock front, on the wall and at the outer edge of the boundary layer. For the carrier phase, we have

$$x=0,\quad \eta>0: u=T=1;$$

$$x\geqslant 0,\quad \eta=0: u=T=a,\quad v=0;$$

$$x>0,\quad \eta\to\infty: u=U_e,\quad T=T_e. \tag{14}$$

Here, U_e and T_e are the velocity and temperature at the outer edge of the gas boundary layer which should be found from the solution of the two-phase flow problem of the relaxation region behind a planar shock wave. For the dispersed phase, we have

$$x>0,\quad \eta=0: u_s=T_s=a,\quad v_s\to 0,\quad n_s v_s=1. \tag{15}$$

The generalization of this problem formulation for a poly-disperse system consisting of m mono-disperse fractions of particles of the same material is obvious: Eqs. (10)—(13) should be solved for each one-velocity continuum of each of m fractions and the source terms Q, R, S should be replaced by the sums $\sum_m\beta_m Q_m$, $\sum_m\beta_m R_m$, $\sum_m\beta_m S_m$, where β_m is the ratio of the velocity relaxation lengths of the m-th fraction and the first fraction whose velocity relaxation length l^* is taken as a reference quantity for normalization. Based on the definition of the phase velocity relaxation length, it is easy to find that, when ρ_s^0 is constant, the parameter β_m depends only on the particle size $\beta_m=(\sigma_m^*/\sigma_1^*)^2$. The mathematical formulation of the problem (6)—(13) contains the following independent similarity criteria: γ, M, Pr, α, χ, κ, ω and Re_0. It should be noted that in the case of poly-disperse particles, each particle fraction will give the corresponding set of the similarity criteria which, in addition, should be complemented by the ratios of the velocity relaxation lengths β_m. It is also worth to note that for very large values of the parameter κ (strictly speaking, when $\alpha\kappa/\sqrt{Re}\sim O(1)$) the self-induced carrier-gas pressure gradient should be taken into account in the near-wall region and the standard "boundary layer plus inviscid flow" scheme fails. However, detailed discussion of this range of parameters lies beyond the scope of the present study.

2 Method of numerical solution for small α case

The main aim of our study was to describe quantitatively the motion of solid particles leaving the surface of the eroded deposit and the structure of the dust cloud formed due to the shear-induced particle entrainment by the laminar gas boundary layer behind the moving shock wave. The general formulation of the problem given in the previous section is too com-

plex for analyzing the mechanism of the aerodynamic entrainment. Thus, in what follows we assume that the mass loading of the dispersed phase is small ($\alpha \to 0$) and the influence of the particles on the carrier-phase parameters can be neglected. This assumption substantially simplifies the procedure of finding the numerical solution, although keeping meaningful the problem formulation since the situation when the mean concentration of entrained particles is fairly small is commonly encountered in practice. In this case, in the system of Eqs. (6)—(13) and the boundary condition (14), we should assume $\alpha = 0$, $p_e = 1/(\gamma M_0^2)$, $U_e = T_e = 1$. The carrier-phase parameters can be calculated separately by using the standard methods of solving the compressible boundary layer problems[15]. For simplicity, we assume that the gas viscosity and thermal conductivity are linear functions of temperature ($\mu^*/\mu_0^* = k^*/k_0^* = T^*/T_0^*$) and $Pr = 1$. Then the standard methods of the pure-gas boundary layer theory make it possible to reduce the problem of calculating the carrier-gas parameters to the boundary-value problem for the Blasius function $f(\xi)$:

$$2f''' + ff'' = 0, \tag{16}$$

$$f(0) = 0, \quad f'(0) = a, \quad f'(\infty) = 1. \tag{17}$$

In our notation, the gas velocity and temperature in the boundary layer can be expressed in terms of $f(\xi)$ as follows:

$$u = f'(\xi), \quad v = -\theta\left[\frac{f}{2\sqrt{x}} + \sqrt{x}f'\frac{\partial \xi}{\partial x}\right],$$

$$T = 1 + \left[\frac{Ec}{2}(1 - a^2) - 1\right](1 - f') + \frac{Ec}{2}(a - 1)(1 - f'^2).$$

Here, the prime denotes differentiation with respect to ξ: $f' = \mathrm{d}f/\mathrm{d}\xi$. A new variable has been introduced:

$$\xi = \frac{1}{\sqrt{x}}\int_0^\eta \rho \mathrm{d}\eta.$$

It is convenient to introduce an auxiliary function ψ, for which the following relations hold:

$$\psi(\xi) = \frac{\eta}{\sqrt{x}} = \int_0^\xi \frac{\mathrm{d}\xi}{\rho} = \int_0^\xi \theta \mathrm{d}\xi,$$

$$\frac{\partial \xi}{\partial x} = -\frac{1}{2x}\frac{\psi}{\psi'} = -\frac{\psi}{2x\theta}.$$

To obtain the gas velocity and temperature, we must first solve the boundary-value problem for the Blasius function $f(\xi)$. Then we obtain the temperature distribution $T(\xi)$, the function $\theta(\xi)$, and hence the function $\psi(\xi)$, in terms of which the relation between the variables η, x and ξ can be expressed. Thus, the numerical solution for $f(\xi)$ at various shock Mach numbers makes it possible to find u, v and T as functions of x and η. As a result, we have the finite difference solution with controlled accuracy for all the parameters of the carrier phase in the boundary layer.

For the dispersed phase, due to the lifting and gravity forces involved, the particle trajectories may intersect. It results in the non-uniqueness of the disperse-phase parameters in the Eulerian coordinates. To avoid the problems associated with intersecting particle trajectories, we introduce the Lagrangian variables (t, x_0), where x_0 is the dimensionless coordinate of the origin of a particle trajectory on the eroded surface and $t = t^* U_0^*/l^*$ is the dimensionless time of particle motion along this trajectory. In the Lagrangian variables, the equations of particle motion take the form:

$$\frac{\mathrm{d}x_s}{\mathrm{d}t} = u_s, \tag{18}$$

$$\frac{\mathrm{d}\eta_s}{\mathrm{d}t} = v_s, \tag{19}$$

$$\frac{\mathrm{d}u_s}{\mathrm{d}t} = \mu(u - u_s)D, \tag{20}$$

$$\frac{\mathrm{d}u_s}{\mathrm{d}t} = \mu(v - v_s)D - \kappa(u - u_s)H\left(\rho\mu\left|\frac{\partial u}{\partial \eta}\right|\right)^{1/2} - \omega. \tag{21}$$

When α is small, the particle temperature has no influence on its motion. That is, there is no coupling between the dynamic and thermodynamic behaviors of the particles. Therefore, for investigating the number-density profiles of the particles in the dust cloud, the equation of the particle temperature can be omitted. In the Lagrangian coordinates (t, x_0), the continuity equation of the dispersed phase for a fixed trajectory can be derived,

$$\frac{1}{n_s(t, x_0)} = |J|,$$

$$J = u_s\frac{\partial \eta_s(t, x_0)}{\partial x_0} - v_s\frac{\partial x_s(t, x_0)}{\partial x_0}. \tag{22}$$

Here, J is the Jacobian of the transformation from the Eulerian to Lagrangian variables. The boundary conditions for the particle motion equations are given below:

$$t = 0: x_s = x_0, \quad \eta_s = 0,$$

$$u_s = a, \quad v_s \to 0, \quad n_s v_s = 1. \tag{23}$$

For determining the particle number density in the cloud n_s from Eq. (22), we must know the values of $\partial x_s/\partial x_0$ and $\partial \eta_s/\partial x_0$. These derivatives can be found by differentiating Eqs. (18)—(21) with respect to x_0:

$$\frac{dw_1}{dt} = w_2, \tag{24}$$

$$\frac{dw_3}{dt} = w_4, \tag{25}$$

$$\frac{dw_2}{dt} = \mu(u - u_s)\frac{\partial D}{\partial x_0} + \mu\left(\frac{\partial u}{\partial x_0} - w_2\right)D + (u - u_s)D\frac{\partial \mu}{\partial x_0}, \tag{26}$$

$$\frac{dw_4}{dt} = \mu(v - v_s)\frac{\partial D}{\partial x_0} + \mu\left(\frac{\partial v}{\partial x_0} - w_4\right)D + (v - v_s)D\frac{\partial \mu}{\partial x_0} - \kappa(u - u_s)\frac{\partial}{\partial x_0}\left[H\left(\rho\mu\left|\frac{\partial u}{\partial \eta}\right|\right)^{1/2}\right] - \kappa\left[H\left(\rho\mu\left|\frac{\partial u}{\partial \eta}\right|\right)^{1/2}\right]\left(\frac{\partial u}{\partial x_0} - w_2\right). \tag{27}$$

In Eqs. (24)—(27), four new functions are defined as

$$w_1 = \frac{\partial x_s}{\partial x_0}, \quad w_2 = \frac{\partial u_s}{\partial x_0}, \quad w_3 = \frac{\partial \eta_s}{\partial x_0}, \quad w_4 = \frac{\partial v_s}{\partial x_0}.$$

The initial conditions for these derivatives introduced above are as follows:

$$t = 0: w_1 = 1, \quad w_2 = 0, \quad w_3 = 0, \quad w_4 = 0. \tag{28}$$

Thus, for the dispersed-phase parameters on a fixed trajectory, we have the closed system of ordinary differential equations (18)—(21), (24)—(27) and algebraic relation (22). This system was solved by the fourth-order Runge-Kutta method for various x_0. In doing this, the values of carrier-gas parameters found on the Euler mesh were interpolated by using second-order polynomials.

The method of solution used here for calculating n_s offers obvious advantages over the widely used ordinary Lagrangian method (see Ref. [16] for example), which requires a very large number of Lagrange trajectories of the particles per Euler cell to ensure satisfactory accuracy of calculating the particle concentration. The discussion on the advantages of the full Lagrangian method can be found in Refs. [17,18].

3 Computation results and discussion

In our calculations, air and aluminum powders are considered respectively as the carrier- and dispersed-phase and the ratio of the gas specific heats $\gamma = 1.4$.

For the case of mono-disperse particles ($m = 1$), some typical trajectories are plotted in Fig. 2 for 1 μm and 10 μm particles respectively at a fixed shock Mach number ($M = 2.0$). It can be seen that the Knudsen effect is significant for finer particles and it can result in increase in the height of particle rise and the distance of particle motion. On the other hand, when the shock Mach number keeps constant, the maximum height of particle entrainment becomes larger not only for the first trajectory but also for all the following trajectories as the particle size increases. The 10 μm particles can even rise out of the gas boundary layer. Fig. 2 also clearly shows that the lifting and gravity forces into account results in the intersection of particles trajectories. In the zone of intersecting particle trajectories, two or more particle trajectories cross over, which leads to the non-uniqueness of the dispersed-phase velocity and other flow parameters.

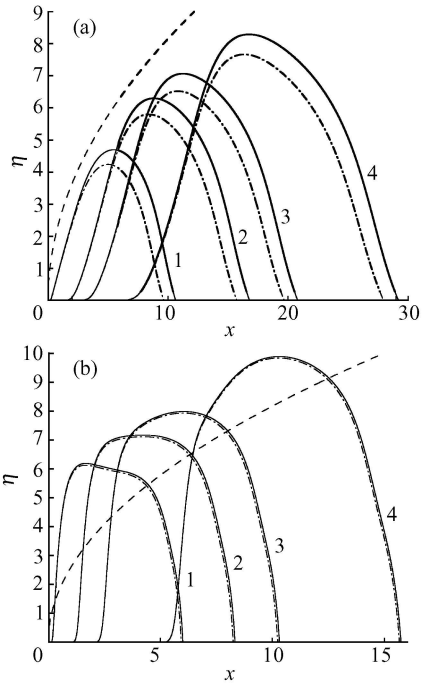

Fig. 2. Effect of the Knudsen number on particle motion at $M = 2.0$. (a) 1 μm particles, curves 1—4 correspond to $x_0 = 0.1$, 1, 2 and 5; (b) 10 μm particles, curves 1—4 correspond to $x_0 = 0.1$, 1, 2 and 5. Solid curves, with the Knudsen effect; chain curves, without the Knudsen effect; broken line, outer edge of the gas boundary layer.

It should be noted that the solution considered is valid only over the length of the laminar flow region which depends mainly on the flow Reynolds number. In the laminar flow region the mode of particle motion may be either saltation-like (for small particles) or purely ascending (for large particles). To determine the dividing boundary between these two modes of particle motion in the plane of the dimensionless particle inertia and lift parameters Re_0 and κ, we performed a parametric study of the particle trajectories originated immediately behind the shock front and found the particle flight distances L over a wide range of the governing parameters ($10 \leqslant Re_0 \leqslant 1000$ and $10 \leqslant \kappa \leqslant 10000$) for the $M = 2.0$ case. The dimensionless coordinate of the transition point $x_c = x_c^*/l^*$ can be expressed as $x_c = Re_c/Re = (6.46Re_0/12\pi\kappa)^4 Re_c$ (Re_c is the flow Reynolds number based on the current dimensional distance from the shock front and the outer flow parameters). In this work, we assume that the critical value of $Re_c = 3.5 \times 10^6$ (see Ref. [15]). Comparing the calculated values of L and x_c for different Re_0 and κ, we found the curve $L - x_c = 0$ which can be considered to be the conventional limit of the saltation mode (Fig. 3). For $M = 2.0$, the saltation-like motion is typical of the 1 μm particles. On the contrary, the motion of the 10 μm particles, even of those located just behind the shock front, will be modified by the turbulence of the gas boundary layer during the descending phase of their trajectories.

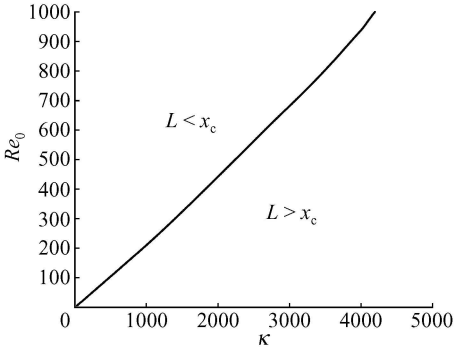

Fig. 3. The Re_0-κ domain for the saltation mode of particle motion at $M = 2.0$.

To estimate the ability of saltating particles to induce the secondary erosion associated with the bombardment of the deposited layer, we calculated the following dynamic properties of the 1 μm particles at impact: the terminal velocities u_{st} and v_{st}, the number fluxes $N_x = n_{st}u_{st}$ and $N_y = n_{st}|v_{st}|$ as well as the momentum fluxes $F_x = N_y u_{st}$ and $F_y = N_y|v_{st}|$. In Fig. 4, these terminal parameters are given as the functions of the distance x from the shock front. Clearly, during their flight in the gas boundary layer, the entrained particles acquire energy from the gas and reach much higher velocities and momentum fluxes when they impact on the deposit surface. Thus, another entrainment mechanism (the so-called bombardment entrainment) may be excited by these energetic impacting particles. The results in Fig. 4 show that, with increase in the distance from the shock front, the terminal number and momentum fluxes (N_x, N_y and F_x, F_y) increase substantially although the magnitudes of the terminal velocities u_{st} and v_{st} vary in a relatively small range, keeping within the same order, and even the absolute value of the terminal normal velocity v_{st} decreases with x. Compared with its initial value at $x \sim 10$, the longitudinal momentum flux F_x at the surface of the deposit layer increases by about one order of magnitude over the laminar flow region ($x \sim 100$). Therefore, the bombardment entrainment may be sustained downstream provided the process of the aerodynamic entrainment of the particles is initiated by the moving front.

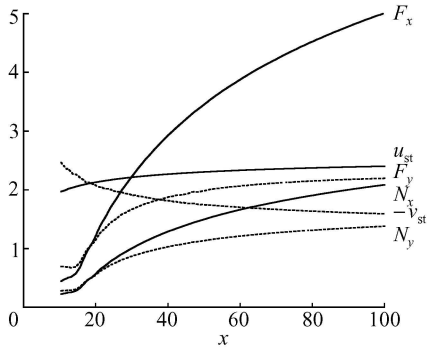

Fig. 4. Development of terminal dynamic properties for 1 μm particles at $M = 2.0$.

In order to study the effect of the shock Mach number on the particle motion, the trajectories originated in the vicinity of the shock front were calculated for four different shock Mach numbers ($M = 1.5$, 2.0, 2.5 and 3.0). For convenience of comparison, the characteristic length l^* and the Reynolds number based on this length at $M = 2.0$ are chosen as the reference scale for normalizing the coordinates x and η in Figs. 5—6. The results shown in Fig. 5 indicate that, as the shock Mach number increases, the parti-

cle rises higher at the early phase of its motion and follows the shock front quicker during the entire period of motion. However, with increase in the shock Mach number, the height of the entrained particle trajectory originated at $x_0 = 0.1$ changes in different trends: it decreases monotonously for the 1 μm particles but varies non-monotonously for the 10 μm particles. Even for those 1 μm particles, initially located far downstream from the shock front (say, at $x_0 = 50$), the trajectory height may not vary in a monotonous way too (Fig. 5(c)).

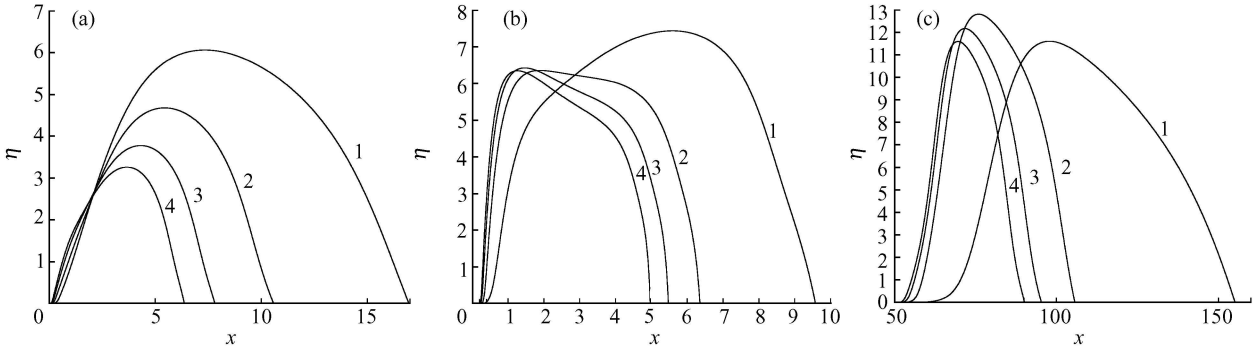

Fig. 5. Effect of the shock Mach number on particle motion. (a) 1 μm particles with the trajectory origin at $x_0 = 0.1$; (b) 10 μm particles with the trajectory origin at $x_0 = 0.1$; (c) 1 μm particles with the trajectory origin at $x_0 = 50$. Curves 1—4 correspond to $M = 1.5$, 2.0, 2.5 and 3.0, respectively.

The dispersed-phase flow patterns of a shock-induced dust cloud involve the collective motion of a mass number of particles. As is well known, the envelope of the trajectory family of all the entrained particles represents the upper boundary of the dust cloud. The effects of the shock Mach number on the shape of the upper boundary of the mono-disperse particles cloud are illustrated in Fig. 6 for the 1 μm and 10 μm particles respectively. In the 1 μm particle case (Fig. 6(a)), the dust cloud thickness increases with the decrease in the shock Mach number over the intermediate region ($\sim 5 < x < \sim 30$). However, this thickness increases with the increase in the shock Mach number in the near-front region ($x < \sim 1$) while it first increases and then decreases with the increase in the shock Mach number in the neighborhood of the laminar-to-turbulent transition point ($x \sim 100$). In the 10 μm particle case (Fig. 6(b)), the laminar-to-turbulent transition occurs at $x \sim 1$ and hence, over the laminar flow region where our model is valid, the dust cloud thickness increases with the increase in the shock Mach number. Fig. 6(b) also shows clearly that, with the increase of the distance from the shock front (say for $x > \sim 5$), the envelop lies higher for lower shock Mach numbers. In other words, multiple factors (not only the shock Mach number but also the particle inertia and lift parameters, and the flow regime, etc.) influence the extension of a shear-induced dust cloud.

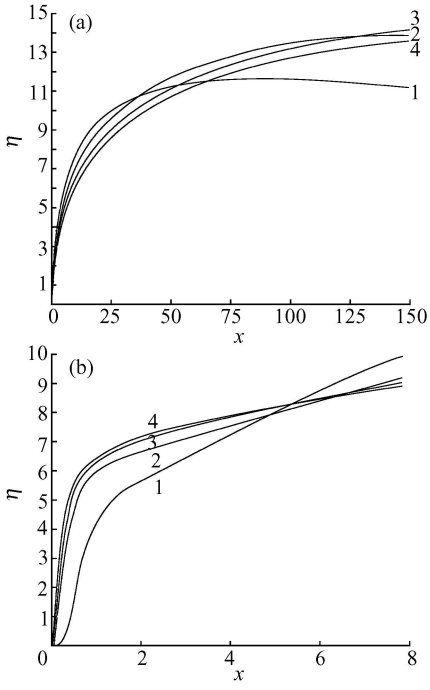

Fig. 6. Effect of the shock Mach number on the envelope of particle trajectories. (a) 1 μm particles; (b) 10 μm particles. Curves 1—4 correspond to $M = 1.5$, 2.0, 2.5 and 3.0, respectively.

For the case of bi-disperse particles ($m = 2$), when the eroded layer consists of 1 μm and 10 μm particles in the ratio of number densities 1:1, the calculated dust-cloud structures are shown in Fig. 7 for the shock Mach number of $M = 1.5$ and 2.0 respectively. In these computations, the impacting particles are assumed to be redeposited on the wall (not re-

bound) and the characteristic length l^* for 10 μm particles and the corresponding Re were chosen for scaling the space coordinates. The obtained results indicate that the upper region of the dust cloud consists of the large 10 μm particles and the lower region of the cloud consists of doubled-sized particles. Obviously, the presence of the small 1 μm particles makes the cloud structure in the lower region more complex. The most important feature is the formation of a multi-layer structure with sharp accumulation of the particles inside the cloud. Since, in our case, the 1 μm particles saltate and their normal velocities vanish on the envelope of the particle trajectories, the number density of the disperse phase grows unboundedly when approaching this envelope and has an integrable singularity there. In the region above the envelope of the 1 μm particle trajectories, the number density of the dispersed phase depends only on the motion of the 10 μm particles. It first decreases sharply and then increases gradually until a larger value is reached at the upper boundary of the cloud, beyond which there exist no particles. It is also found that the number density of the dispersed phase takes its maximum value on the deposit-layer surface due to the vanishing normal velocity. The stratification phenomenon discussed is a new feature for a poly-disperse system. In the case of bi-disperse particles under consideration there is one sharp accumulation zone inside the cloud, except for those high-density zones near the deposited surface and upper boundary of the cloud. It is easy to determine that the number of particle accumulation zone is equal to $(m-1)$ for more general cases of poly-disperse systems ($m \geqslant 3$).

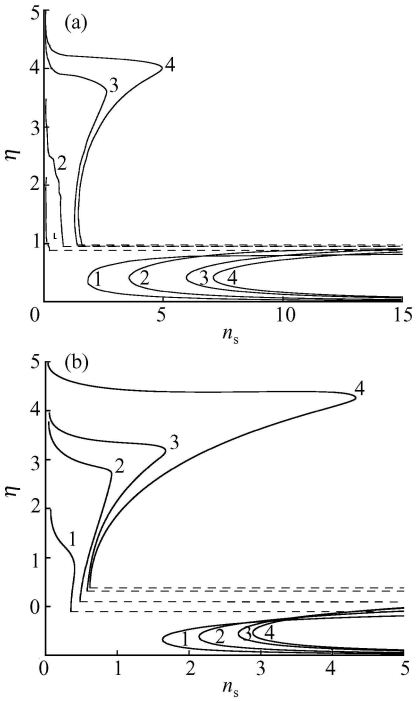

Fig. 7. Spatial development of the dust-cloud structure in the bi-disperse system. (a) Mach number $M=1.5$; (b) Mach number $M=2.0$. Curves 1—4 correspond to $x=0.2$, 0.4, 0.8 and 1.0, respectively.

4 Summary

Dust-cloud structures behind a shock wave moving over a deposited layer of fine particles are studied numerically. The usual two-fluid model of dilute dusty gas is modified with account for poly-dispersity of the particles. In addition, this model takes into account the possibility of intersection of particle trajectories due to the action of the shear lifting force and the gravity. The numerical simulation indicates that the presence of the gas boundary layer behind a moving front (such as a shock wave) ensures the incipience of particle entrainment from the surface into the air, due to the aerodynamic mechanism. Our calculations show that the Knudsen effect should be taken into account when the diameter of a particle is about 10 μm; otherwise the thickness of the dust cloud may be underestimated.

The entrainment capacity of the shock-induced boundary layer depends on the particle inertia and the shock Mach number. Our calculations show that, due to the action of the lifting force, the height of particle rise increases with the increase in particle size and the particles of about 10 μm in size may be even ejected out from the carrier-gas boundary layer. With the increase in the shock Mach number, the particles rise faster at the initial phase of their entrainment but the height of their rise, in general, decreases except for those particles initially located far downstream. The extension of the shear-induced dust cloud displays non-monotonous behavior and depends multiple factors, including the shock Mach number, the particle inertia and lift parameters, and the flow regime.

The obtained results indicate that the non-uniformity of the particle size in the deposited layer leads to the onset of sharp stratification of the dispersed phase and the formation of local particle accumulation zones inside the dust cloud. The formation of these zones of high particle concentration in the near-wall region behind a moving shock wave may be important for estimating the concentration limit of non-explosivity of dust-gas mixtures and other relevant problems.

References

1 Bielert U. and Sichel M. Numerical simulation of dust explosions in pneumatic conveyors. Shock Waves, 1999, 2: 125—139.

2 Zhang F., Gronig H. and van de Ven A. DDT and detonation waves in dust-air mixtures. Shock Waves, 2001, 11: 53—71.

3 Batt R. G., Petach M. P., Peabody II S. A. et al. Boundary layer entrainment of sand-sized particles at high speed. J. Fluid Mech., 1999, 392: 335—360.

4 Osiptsov A. N. Mathematical modeling of dusty-gas boundary layers. Appl. Mech. Rev., 1997, 50: 357—370.

5 Merzkirch W. and Bracht K. The erosion of dust by a shock wave in air: initial stage with laminar flow. Int. J. Multiphase Flow, 1978, 4: 89—95.

6 Hwang C. C. Initial stage of the interaction of a shock wave with a dust deposit. Intl. J. Multiphase Flow, 1986, 12: 655—666.

7 Wu Q. and Wang B. Y. Numerical analysis of dust particle entrainment induced by shock waves. In: Proc. 2-nd Intern. Symp. on Intense Dynamic Loading and Its Effects. (ed. Zhang G. R.) Chengdu: Sichuan University Press, 1992, 167—170.

8 Wang B. Y. and Osiptsov A. N. Near-wall boundary layer behind a shock wave in a dusty gas. Izv. Ross. Akad. Nauk, Mekh. Zhidk. Gaza, 1999, 4: 61—73; Engl. Transl.: Fluid Dynamics, 1999, 4: 505—515.

9 Bazhenova T. V. and Gvozdeva L. G. Unsteady Interaction of Shock Waves (in Russian). Nauka, Moscow, 1977.

10 Marble F. E. Dynamics of dusty gases. Annu. Rev. Fluid Mechanics, 1970, 2: 397—446.

11 Carlson D. J. and Hoglund R. F. Particle drag and heat transfer in rocket nozzles. AIAA Journal, 1964, 2: 1980—1984.

12 Fuchs N. A. Mechanics of Aerosols. New York: MacMillan, 1964.

13 Mei R. An approximate expression for the shear lift force on a spherical particle at finite Reynolds number. Int. J. Multiphase Flow, 1992, 18: 145—147.

14 Saffman P. G. The lift on a small sphere in a slow shear flow. J. Fluid Mech., 1965, 22: 384—400; and Corrigendum. J. Fluid Mech., 1968, 31: 624.

15 Schlichting H. Boundary Layer Theory (7th edition). New York: McGraw-Hill, 1979.

16 Crowe C. T. Review-numerical models for dilute gas-particle flows. ASME J. Fluid Eng., 1982, 104: 297—303.

17 Osiptsov A. N. Lagrangian modelling of dust admixture in gas flows. Astrophys. Space Sci., 2000, 274: 377—386.

18 Healy D. P. and Young J. B. Calculation of inertial particle transport using the Osiptsov Lagrangian method. ICMF2001, New Orleans, LA, USA, May 27-June 1, 2001, CD, 1—12.